creative commons
COMMONS DEED

저작자표시 2.0 대한민국

이용자는 아래의 조건을 따르는 경우에 한하여 자유롭게

- 이 저작물을 복제, 배포, 전송, 전시, 공연 및 방송할 수 있습니다.
- 이차적 저작물을 작성할 수 있습니다.
- 이 저작물을 영리 목적으로 이용할 수 있습니다.

다음과 같은 조건을 따라야 합니다:

저작자표시. 귀하는 원저작자를 표시하여야 합니다.

- 귀하는, 이 저작물의 재이용이나 배포의 경우, 이 저작물에 적용된 이용허락조건을 명확하게 나타내어야 합니다.
- 저작권자로부터 별도의 허가를 받으면 이러한 조건들은 적용되지 않습니다.

저작권법에 따른 이용자의 권리는 위의 내용에 의하여 영향을 받지 않습니다.

이것은 이용허락규약(Legal Code)을 이해하기 쉽게 요약한 것입니다.

Disclaimer

dCollection

工學碩士學位論文

Fabrication of CVD-grown graphene/Ag nanocomposites and its flexible sensor application

그래핀/은 나노복합체의 제조와
플렉서블 센서의 응용

2013年 2月

서울大學校 大學院
化學生物工學部
俞 善 我

↑
2cm
↓

Fabrication of CVD-grown graphene/Ag nanocomposites and its flexible sensor application

2013

俞善我

↑
2.5cm
↓

↑
4cm
↓

↑
3cm
↓

↑
2cm
↓

학위논문 원문제공 서비스에 대한 동의서

본인의 학위논문에 대하여 서울대학교가 아래와 같이 학위논문 제공하는 것에 동의합니다.

1. 동의사항

① 본인의 논문을 보존이나 인터넷 등을 통한 온라인 서비스 목적으로 복제할 경우 저작물의 내용을 변경하지 않는 범위 내에서의 복제를 허용합니다.

② 본인의 논문을 디지털화하여 인터넷 등 정보통신망을 통한 논문의 일부 또는 전부의 복제.배포 및 전송 시 무료로 제공하는 것에 동의합니다.

2. 개인(저작자)의 의무

본 논문의 저작권을 타인에게 양도하거나 또는 출판을 허락하는 등 동의 내용을 변경하고자 할 때는 소속대학(원)에 공개의 유보 또는 해지를 즉시 통보하겠습니다.

3. 서울대학교의 의무

① 서울대학교는 본 논문을 외부에 제공할 경우 저작권 보호장치(DRM)를 사용하여야 합니다.

② 서울대학교는 본 논문에 대한 공개의 유보나 해지 신청 시 즉시 처리해야 합니다.

논문제목: 그래핀/은 나노복합체의 제조와 플렉서블 센서의 응용

학위구분 : **석사** □ · **박사** □
학 과 : 화학생물공학부
학 번 : 2011-21050
연 락 처 :
저 작 자 : 유 선 아 인)
제 출 일 : 2013 년 1 월 11 일

서울대학교총장 귀하

Abstract

Fabrication of CVD-grown graphene/Ag nanocomposites via and its flexible sensor application

Sun ah You
School of Chemical and Biological Engineering
The Graduate School
Seoul National University

The fabrication of designable CVD-grown few-layer graphene is a promising research area for enhanced device performance. In this study, the few-layer graphene was grown on Cu foil by chemical vapor deposition (CVD) method and functionalized with oxygen plasma treatment under controlled conditions, such as exposure time, input power and distance between the graphene and the plasma electrode. Oxygen plasma treated few-layer graphene (OPFG) results in high

surface energy, leading to effectively attracting Ag+ ions in electrostatic interactions. Interestingly, the distribution of the metal nanoparticles increased with increasing the exposure time and their diameters were controlled by UV irradiation. Uniform Ag nanoparticles (Ag NPs) with ca. 9 nm diameter were successfully decorated on the graphene surface. Moreover, the Ag NPs/OPFG nanocomposite (AgNP–G) film has excellent mechanical bendability and durability in a flexible system. Furthermore, flexible hydrogen sensor of AgNP-G showed highly sensitive and reversible at room temperature (Minimum detection level, ca. 40 ppm)

Keywords: Graphene nanocomposites, CVD-grown graphene, Oxygen plasma, Flexible sensor

Student Number: 2011-21050

Contents

List of Figures

List of Tables

Chapter 1. Introduction

1.1 Graphene nanocomposites

Graphene nanocomposites with well-designed nanostructure using polymer, metal or semiconductors have been extensively fabricated in order to improve mechanical, optical or electrical properties [1-4]. As a robust template for decoration of nanomaterials, Graphene, a two-dimensional single carbon network, has amazing properties including high charge mobility, high mechanical strength, and high electrical and thermal conductivity arising from its hexagonal lattice structure [5-8]. Moreover, conductive graphene layer in graphene nanocomposites can serve as a platform for fast charge transportation.

In this respect, several strategies to incorporate the graphene sheets in a composite material have been studied to take advantage of these outstanding properties of the graphene. As general approaches for fabrication of graphene nanocomposites, graphene oxide (GO) with various functional derivatives, chemically modified reduced graphene

oxide (RGO), or surface functionalized chemical vapour deposition (CVD)-grown graphene are utilized to prepare nanocomposites via simple mixing process, electrochemical deposition, or electroless deposition[5,8]. For graphene/polymer nanocomposites, enhancement of mechanical strength, degradation stability, rheological and permeability properties based on its robust structure can be expected [12]. In addition, graphene/metal nanocomposites exhibit excellent properties including novel catalytic, magnetic and optoelectronic characteristics for use of electronic devices [13].

Significantly, graphene nanocomposites-based devices has attracted great attention in the energy and environmental application areas [1, 2]. In particular, its application, such as supercapacitors, chemical and biochemical sensors, and catalysis has been improved by synergistic effect of graphene nanocomposites.

1.1.1 Synthetic methods of graphene/metal nanocomposites

Graphene/metal nanocomposites represent interesting alternatives

for development of efficient, fast and low-cost devices in electrical technologies [3-6]. Recently, a wide range of researches in synthesis of graphene-metal nanocomposites have been conducted, for example, chemical mixing, electrochemical, and electroless deposition using graphene oxide (GO) which was oxidized from graphite by chemical exfoliation or CVD-grown graphene [7].

Especially, various modified functional components of the GO make it possible to anchor the diverse metallic nanoparticles onto the graphene surface, and chemical reduction process restore the graphitic network of sp^2 bonds, from GO to RGO, with increasing conductivity [8, 9]. However, the synthetic method using GO involve highly toxic chemicals, such as hydrazine hydrate or hydroquinone, and high temperature.

For decoration method of metal nanoparticles on the CVD-grown graphene, the graphene/metal nanocomposites has been conducted by conventional electrochemical or electroless deposition to utilize the difference in potential energy between target metal ions and counter

metal [18, 19]. As CVD-grown graphene in graphene/metal nanocomposites has scalability and adjustability of the graphene layers, the composites can be fabricated as ultra thin film with different sizes. On the other hand, difficulties of mass production and high price limit availability for use of CVD-grown graphene.

1.1.1.1 Graphene oxide (GO)/metal nanocomposites

Wet-chemical method to synthesize the graphene oxide (GO)/metal nanocomposites has employed functionalized graphene with variable sp^2/sp^3 fractions to decorate the metal nanoparticles. it is significantly essential to functionalize the surface of graphene or utilize the GO with oxygenated functional groups because vacancies or strains resulting from defects of the graphene stabilize the metal clusters [20].

Well-known synthesis is mainly simple physical blending between GO and metal nanoparticles or reduction process of metal precursors by using strong reducing agents and increasing reaction temperature. For instance, metal precursors, such as $AgNO_3$, K_2PtCl_4, $HAuCl_4$, were added into functionalized GO solution with reducing agents, $NaBH_4$,

poly(*N*-vinyl-2-pyrrolidone), hydrazine, and stabilizer [5, 8]. This chemical reduction process makes it possible to fabricate large quantity of composites, but removing impurities, such as sulfuric/nitric acid or hydrazine, is still a challenge, leading to low electrical performance of graphene/metal nanocomposites. Another approach to fabricate the nanocomposites is electrochemical reduction, which is to apply electrode potential in order to overcome the energy barriers of target materials [53]. This method has advantage of fast reaction and free-contamination compared to chemical reduction method. However, electrochemical method has space restraints as external power source is necessary.

1.1.1.2 CVD-grown graphene/metal nanocomposites

CVD-grown graphene is a great important material due to its outstanding properties in terms of optical transparency and electrical conductivity [10, 11]. Importantly, while reduction of GO sheets in aqueous solution results in agglomeration, CVD-grown graphene synthesized by gas in vacuum enables the growth of ultra-thin films to

minimize contact resistance and improve charge mobility [14, 15].

Electrochemical or electroless deposition method occurs spontaneously under required condition which is that reduction potential of metal should be higher than one of graphene supported substrate, such as copper [18, 19]. Moreover, UV assisted reduction of metal ion precursors has been recently reported [41]. The UV irradiation induced photolysis caused reduction of metal ions on the surface of the graphene [22, 23].

1.1.2 Application of graphene/metal nanocomposites based flexible sensor

Graphene/metal nanocomposites fabricated from various synthetic methods using graphene oxide or CVD-grown graphene have been widely utilized as building blocks for electrical application, photovoltaics, memory device, and sensor [3-6]. Recently, its outstanding properties including high surface area, high electronic conductivity and bendability with stable state under flexible system lead to flexible sensor application.

The flexible sensors have attracted a great deal of interest in ultra-sensitive semiconductors based on flexible plastic substrates. This new area requires biocompatibility, flexibility, mechanical resistance, and lightweight. Furthermore, flexible sensor based on CVD-grown graphene has a high capability for sensing compared to GO due to high electron mobility and high conductivity resulting from low contact resistance between horizontally located-graphene with thin layers.

1.2 Objective of this study

We provide a facile and reliable synthetic route for fabricating the designable metal NPs-decorated CVD-grown few-layer graphene through surface engineering. Specifically, the surface characteristic of the graphene was modified with controlled conditions, such as plasma exposure time, input power, and distance between the plasma electrode and the sample. The surface of the oxygen plasma treated graphene has oxygen-containing groups including carboxylic acid (-COOH) and hydroxyl (-OH), leading to trap sites to attract the Ag^{+} ions in

electrostatic interactions [21]. Consecutively, UV irradiation was carried out to reduce Ag metal nanoparticles (Ag NPs) with high crystalline and uniform sizes under photo-reduction mechanism [22, 23]. Interestingly, it is noticeable that population of Ag NPs increases with increasing the degree of plasma oxidation, leading to high surface energy. Additionally, the AgNPs-decorated few-layer graphene (AgNPs-G) nanocomposites showed excellent bendability and mechanical durability in flexible systems. As its application, flexible hydrogen sensor of AgNPs-G showed highly sensitive and reversible at room temperature.

Chapter 2. Experimental

2.1 Materials

CVD-grown graphene was synthesized from H_2, CH_3 and Ar gases (99.99%, Daesung Industrial Gases Co. South Korea). Cu foil and flexible polyethylene-terephthalate (PET) film (Aldrich chemical Co) were employed as the graphene substrate. Poly (methylmethacrylate) (950 PMMA A4, 4% in anisole, MicroChem Corp., USA) was used as a medium of transferring the graphene. Silver nitrate (98% $AgNO_3$) was obtained from Aldrich Chemical Co and used without further purification. Silver nitrate solutions were prepared in deionized water.

2.2 Preparation of CVD-grown few-layer graphene

Graphene was grown on 25-μm-thick Cu foil with CH_4 gases as the carbon source by chemical vapor deposition (CVD) method. In a typical growth process, the Cu substrate was heated to 1000 ^oC and H_2 gases (with flow rate of 8 sccm) were maintained to 90 mtorr under evacuated atmosphere for 30 min. Then 20 sccm of CH_4 were introduced for 40 min at a total pressure of 560 mTorr. Finally, the Cu foil was cooled to room temperature at the rate of 35 °C/min under H_2 environment. After the growth of pristine graphene, polymethylmethacrylate (PMMA) solution dissolved by 4% anisole was spin-coated at the rate of 5000 rpm for 1 min. The PMMA-coated graphene was immersed into Cu etchant and the detached graphene was transferred to the flexible substrate (PET film). The residual PMMA was removed by acetone. After the CVD process, the gold electrode was deposited on the dried graphene films by electron beam.

2.3 Surface engineering of graphene

The graphene were exclusively treated using the oxygen plasma equipment (MYPL-200 from APP Co-Ltd, South Korea). A portion of each transferred graphene sample was directly exposed to oxygen/argon (2:800) plasma; exposure time, input power, and distance. Between the graphene surface and the plasma was varied: exposure times of 5, 10, 15, and 20 s, input powers of 100, 150, and 200 W, and distances of 5, 8, and 11 mm were used.

2.4 Synthesis of graphene decorated with Ag nanoparticles

Silver nanoparticles were decorated on the oxygen plasma-treated few-layer graphene (OPFG) by UV-lamp (Matsushita UV system, South Korea). Specifically, the glass chamber (0.5 x 1.0 cm) was attached to the surface of the OPFG. Then, 100 μL of 2 wt% silver nitrate solution were added to the glass chamber, and the sample was exposed to UV light (input power, 300 W) as one of Ag-reduction

methods for 10 min. Residual Ag NPs were removed by washing with distilled water. The AgNPs-G was dried under a vacuum atmosphere at 60 °C for 24 h.

2.5 Electrical measurement of sensitivity in AgNPs-G sensor

Electrical measurements were conducted with a Keithley 2400-SourceMeter and a Wonatech WBCS 3000 potentiostat. The graphene circuit decorated with Ag NPs was mounted in a test chamber (1000 mL) equipped with a gas inlet/outlet and electrical feed-through. Mass Flow Controllers (MFCs, SEC 4400 from KNH) were connected to the hydrogen (the analyte) and nitrogen gas. The nitrogen gas served to dilute the hydrogen gas, thereby providing a low-concentration of the analyte, and to remove the residual hydrogen gas adsorbed on the sample.

To investigate the sensitivity of the AgNPs-G hydrogen sensor, the chamber was first flushed with high-purity N_2 repeatedly to reach the

steady electrical resistance. Then, a predetermined amount of hydrogen was injected into the test chamber through a syringe. The test chamber was periodically flushed with a H_2/N_2 stream in order to estimate the reproducibility and reversibility of the sensors. The concentration of hydrogen gas was changed by controlling the nitrogen and hydrogen flow rates. The sensitivity of the AgNPs-G was calculated by measuring the normalized electrical resistance change, $\Delta R/R_0 = (R - R_0)/R_0$, where R_0 and R are the measured real-time resistance and initial resistance, respectively. The response time was determined as the time required for the conductance to reach 90% of the equilibrium value. The recovery time was the time necessary for the sensor to achieve a conductance 10% above its original value.

2.6 Characterization

Fabricated Pristine graphene (PG) and OPFG were characterized by Raman and X-ray Photoelectron Spectra (XPS) which were recorded on a LabRAM HR (Sci-Thch instrument Co. Ltd) with 1064 nm laser

excitation and an AXIS-His (KRATOS), respectively. Analysis of static contact angle for modified graphene was carried out using a DSA 100 drop shape analysis sytem (Kruss GmbH). The AgNPs-G were characterized by transmission electron microscope (TEM) obtained from a JEOL JEM-200CX. High-resolution transmission electron microscopy (HR-TEM) was also introduced to confirm Ag NPs (JEOL JEM-3010). The PG and AgNPs-G were analyzed using a gold grid purchased from Woo Myoung Incorporation. The surface morphology of the sample was observed using an atomic force microscope (AFM, Nanoscope IIIa, Digital instruments, USA). AFM topographic analysis was conducted in the tapping mode using silicon tips with a resonance frequency of 320 kHz. All electrical measurements for flexible AgNPs-G circuit array were conducted with a Keithley 2400-SourceMeter and a Wonatech WBCS 3000 potentiostat.

Chapter 3. Results and discussion

3.1 Fabrication of OPFG and its characterization

3.1.1 Mechanism of functionalization on graphene surface

Generally, the structural defects and disorder of graphene can be induced by plasma treatment; hence few layer graphene (FLG) was chosen for the fabrication of AgNPs-G nanocomposites. The FLG film was exposed to oxygen plasma to oxidize the graphene surface. The plasma directly generates excitation of oxygen atoms produced by the following ways [24].

$$e + O_2 \rightarrow e + O^* + O \quad (1)$$

$$e + O_2 \rightarrow e + 2O^* \quad (2)$$

Moreover, it has been reported that the presence of Ar enhances the content of active oxygen owing to the production of oxygen atoms by the quenching reaction [25]. Metastable Ar atoms react with the

oxygen molecules which are subsequently dissociated into active oxygen. At the same time, radicals are generated from the double carbon bonds broken by plasma treatment because active π bonds in C=C are susceptible to plasma attack [26]. Then, highly active oxygen readily bond to unstable radicals in carbon atoms to maintain the octet rule. The possible reaction mechanism is believed to produce the oxygen-containing functional groups, such as hydroxyl, carbonyl or carboxyl (C-OH, C=O or HO-C=O) through stabilization with hydrogen atom [27, 28]. The hydrogen atom can be introduced *via* atmosphere absorption.

3.1.2 Raman and XPS analysis of OPFG film with different plasma treatment factors

A Raman spectroscopy is efficient analysis method for demonstrating the defect and the layer number of graphene through the D, G and 2D bands. Figure 1 shows the evolution of Raman spectra according to the plasma exposure time. The D band, A_{1g}

breathing mode, is associated with the extent of defects in the curved graphite sheet, sp^3 carbon, or other impurities. The G band results from first-order scattering of the E_{2g} mode in sp^2 carbon domains, corresponding to the opposite direction movement between two neighboring carbon atoms [29, 30]. In addition, the second-order two phonon mode (2D band, at 2708 cm^{-1}) is a definite criterion to distinguish graphene from other amorphous carbon materials [31]. The number of layers of graphene was determined by comparing its relative intensity of the G peak [32]. For PG, the G peak is located at 1580 cm^{-1} in figure 1a, and no trace of D peak is observed. Defect-free graphene exhibits a sharp and symmetric 2D peak at 2708 cm^{-1}. Also, the full width at half-maximum (FWHM) of the G peak is 15 (±1) cm^{-1} in inset of figure 1b. The sharp G peak (low value of FWHM) indicates good uniformity of the PG. The surface of the graphene was oxidized for different treatment times (5, 10, 15 and 20 s). After the exposure for 5s, the D peak appeared at 1350 cm^{-1} with decreasing G and 2D peaks. Moreover, the intensity ratio of the D and G bands

(I_D/I_G) is a measuring stick to evaluate the quality of the graphene as it is directly related to the diameter of the crystalline cluster in the graphene [33]. Notably, the diameter of crystalline region is well-known to be inversely proportional to *I(D)/I(G).*The value of I_D/I_G increased from 0.16 to 0.8 with increasing oxygen plasma treatment time (3 to 20 s), leading to decrease in the number of sp^2 ordered rings. In particular, D′ peak of OPFG 20 was originated from the disorder-induced double resonance Raman scattering process or defect regions, resulting in vacancy formation as defect in graphene structure [34]. The surface engineering for up to 20 s increased the density of the structural defects, judging from the broadened D, G peaks and the increased I_D/I_G values.

Furthermore, figure 2 displays the Raman spectra with varying input power (100 to 200 W, 5 s, 8 mm) and distance between the graphene and plasma electrode (5 to 11 mm, 5 s, 150 W), respectively. The surface of graphene treated by oxygen plasma at 100w displays no detectable defect from Raman measurement (Figure 2a). This

means that input power of 100 W is weak to functionalize the graphene. However, increase of input power generates more lattice defects, judging from increase of the intensity ratio of *I(D)/I(G)* and D peak in table 1. In figure 2b, D and D′ peaks at 1350 and 1621 cm^{-1} were observed in the sample treated at a distance of 5 mm. Specifically, the D and D′ peaks are known to be activated by defects and disorders, indicating that oxygen plasma treatment at 5 mm generates oxygen-related defects with conversion of carbon atom from sp^2C to sp^3C. Moreover, the spectra in terms of distance variation shows significant change with increase of D and D′ peaks compared to the spectra of input power. Therefore, it can be expected that distance is a more influential factor to modify the graphene surface.

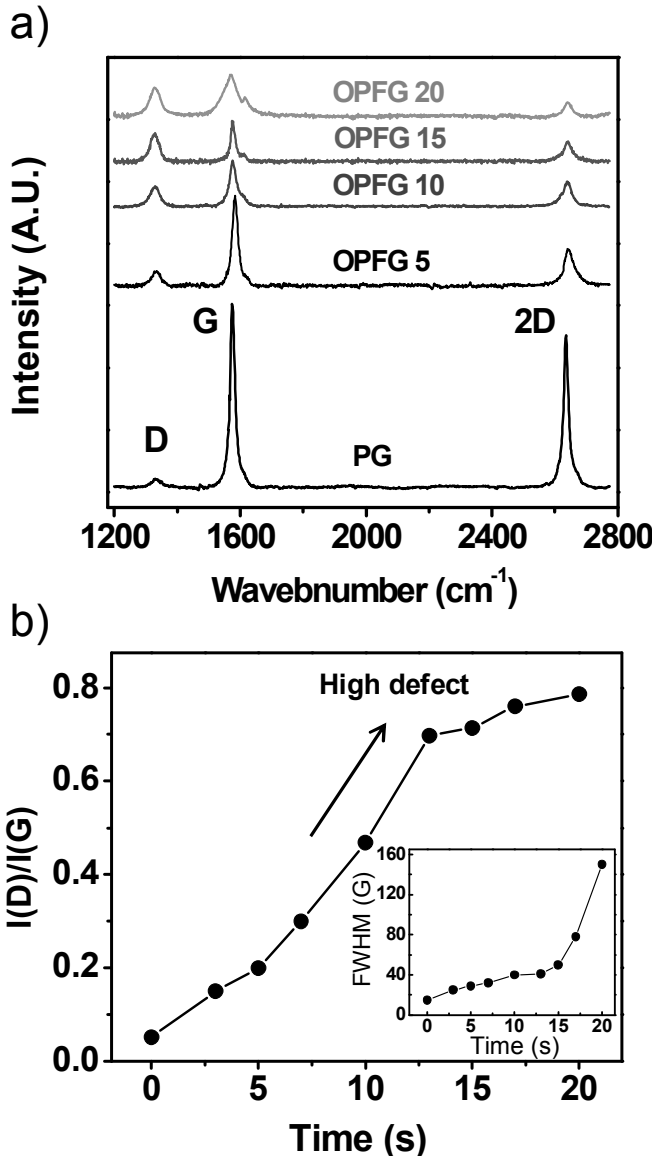

Figure. 1 (a) Raman spectra of the PG and OPFG as a function of exposure time (5, 10, 15, and 20 s). (b) Intensity ratio of D/G (inset shows full width at half-maximum of G peak; FWHM (G).)

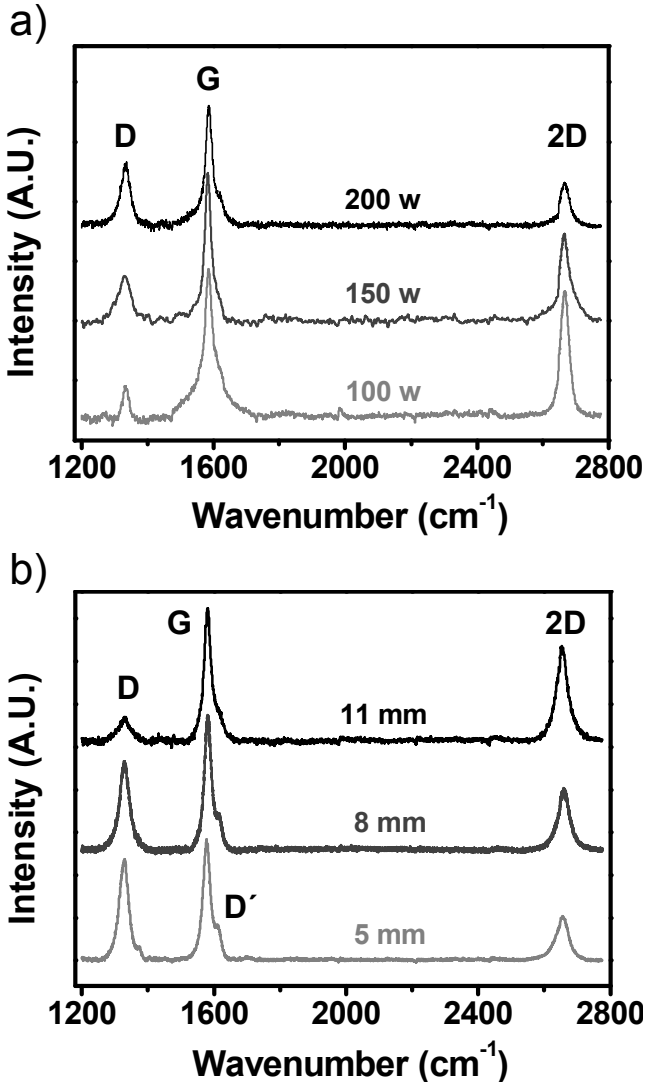

Figure. 2 Raman spectra of OPFG according to (a) input power (100, 150, and 200 w) and (b) distance between the graphene and plasma electrode (5, 8, and 11 mm).

Table. 1 Raman intensity ratio of D, G, and 2D and I(D)/I(G) in terms of oxygen plasma treatment based on three variables including exposure time, input power and distance between the graphene and the electrode.

Plasma treatment	**Condition**	**D***	**G***	**2D***	***I(D)/I(G)***
Exposure time	5 s	1.30	0.64	0.38	0.20
	10 s	3.16	0.36	0.23	0.47
	15 s	4.07	0.31	0.20	0.70
	20 s	6.51	0.20	0.11	0.79
Distance	5 mm	5.61	0.65	0.38	0.86
	8 mm	3.25	0.77	0.52	0.65
	11 mm	1.25	0.93	0.91	0.17
Input power	100 w	1.15	0.96	0.92	0.19
	150 w	1.60	0.81	0.78	0.37
	200 w	2.45	0.69	0.43	0.62

D*, G* and 2D* are the intensity ratio of *Plasma treatment with three variables/Few layered pristine graphene*.

X-ray photoelectron spectroscopy (XPS) provided further information about the presence of oxygen-containing groups. The C 1s peak centered at 284.3 eV (Figure 3) represents sp^2C-sp^2C that is originated from a benzene ring. OPFG had a broad C 1s peak due to a considerable oxidation degree with three components: 286.5 eV for O-sp^3C, 287.3 eV for OH-sp^3C, and 288.4 eV for O-sp^2C bonds [35, 36]. By increasing oxygen exposure time, the high resolution spectra of C 1s in various OPFG in figure 3 shows increase of sp^3C-sp^3C peaks at 285.1 eV attributed to defects on the graphene and shoulder peaks related to oxygenated carbon atoms, whereas sp^2C-sp^2C peaks (C=C) decrease in the spectra of OPFG. To gain some insight into OPFG 20, it is found that the surface oxidation could be considered to almost reach to a saturation state of C-O_x groups as no dramatic changes of functional groups was shown in the OPFG 20 [25]. Moreover, figure 4 shows the atomic contents of OPFG as a function of exposure time. As

oxygen plasma exposure time increased, the contents of oxygen atom increased and the carbon atomic contents decreased. These results represent that oxygen plasma treatment causes oxidation of the C=C bonds on the surface of the graphene at the same time as generation of various functional groups ($C\text{-}O_x$).

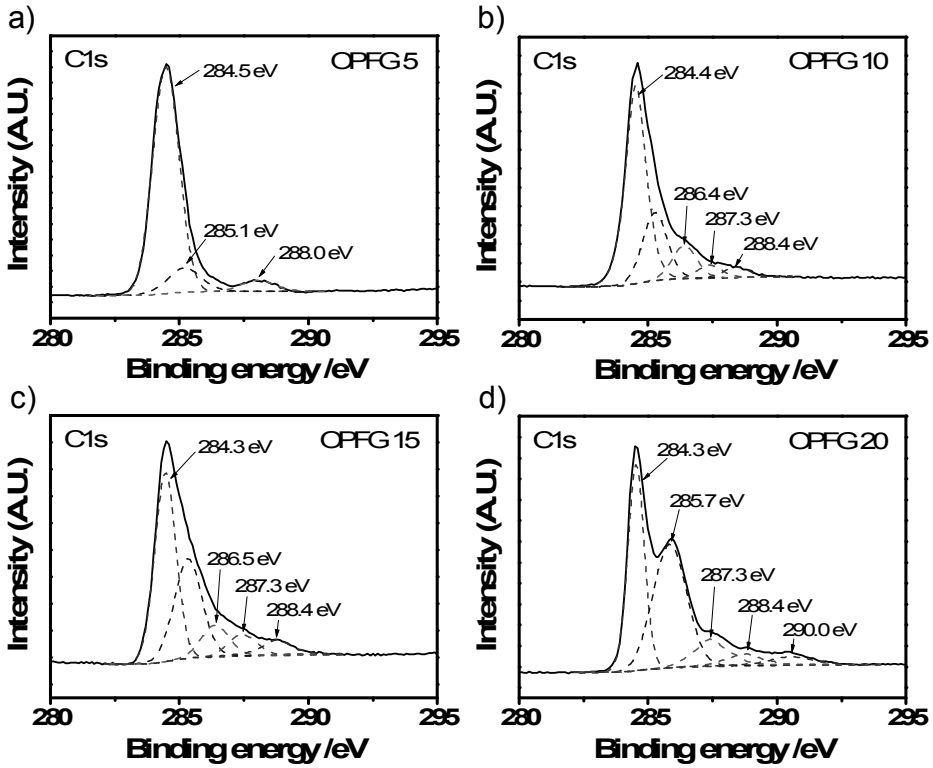

Figure. 3 XPS spectra of high resolution of C1s for (a) OPFG 5, (b) OPFG 10, (c) OPFG 15, and (d) OPFG 20.

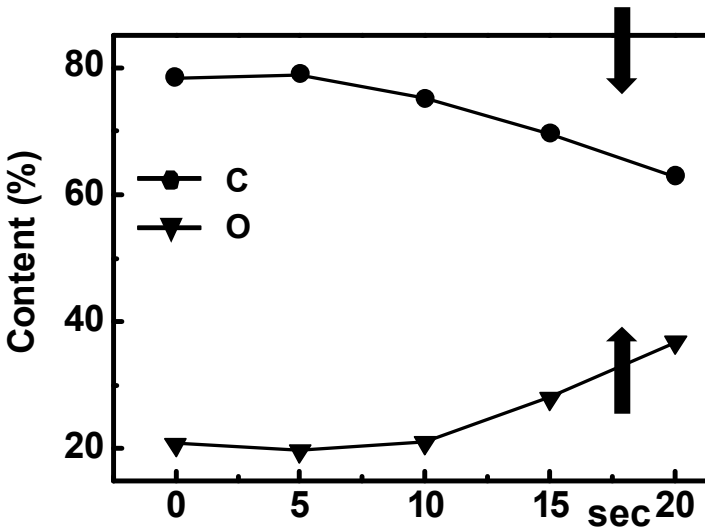

Figure. 4 Content changes in oxygen and carbon atom as the oxygen plasma exposure time increases.

3.1.3 Surface energy analysis of OPFG film with different plasma treatment time

To achieve an in-depth insight into the surface characteristic of OPFG, static contact angles were measured by using water and diiodomethane on the OPFG film at room temperature. Figure 5 shows the change of water contact angle on the surface of the OPFG with different exposure times. PG on PET film had 88.1 °±0.09 in equilibrium contact angle. After plasma surface modification, decrease in the contact angle of OPFG indicates the increase in the amount of oxygen-containing functional groups. Moreover, the surface energies, which are the sum of dispersive and polar fractions [37], were calculated with contact angle data in table 2, leading to dramatic increase of surface energies from 38.17±0.21 of PG to 65.28±0.18 mJ/m^2 of OPFG 20 shown (Figure 6). For this reason, high surface energy of OPFG attributed to the existence of polar functional groups on the surface plays a crucial role in good adhesiveness with charged materials, such as metal ions [38].

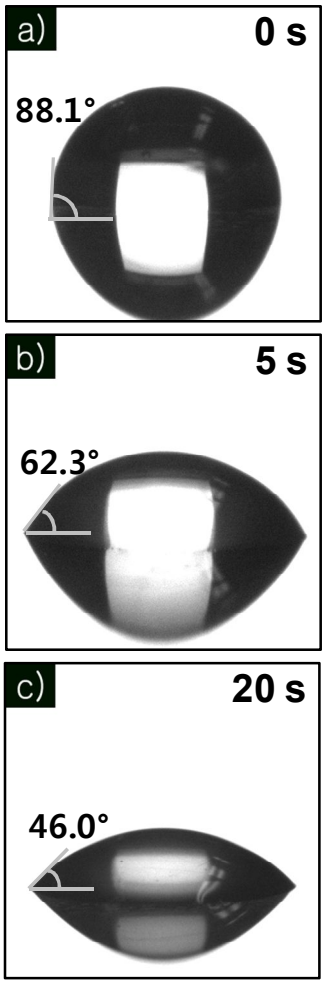

Figure. 5 Contact angle on the surface of (a) pristine graphene, oxygen plasma treated graphene (b) for 5 s and (c) for 20 s. All samples were transferred on flexible PET film.

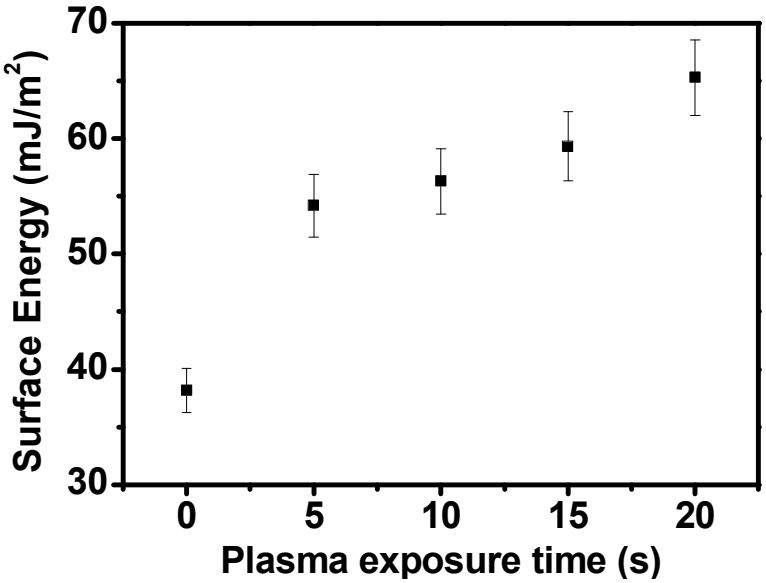

Figure. 6 Surface energy of OPFG film as a function of plasma exposure time at room temperature; Total surface energy is known to be the sum of dispersive and polar fractions.

Table. 2 Contact angle of water and diiodomethane (CH_2I_2) on OPFG film at different oxygen plasma exposure time.

Exposure time [s]	θ_{water} [°]	$\theta_{Diiodomethane}$ [°]
0	88.1±0.09	41.9±0.02
5	62.3±0.20	32.2±0.02
10	60.2±0.19	28.8±0.01
15	54.7±0.08	26.8±0.15
20	46.0±0.15	20.0±0.01

3.2 Fabrication of AgNPs-G and its characterization

The overall synthetic procedure for Ag nanoparticles-decorated graphene (AgNPs-G) is illustrated in figure 7. CVD-grown graphene was transferred on the PET film, and gold-patterned electrode was deposited on the graphene in order to fabricate a flexible graphene circuit array. Then, oxygen plasma-based surface engineering functionalized the graphene surface. Generated oxygen-containing groups attract added silver ion through electrostatic interaction. Uniform Ag nanoparticles (Ag NPs) on the surface of OPFG were formed by simple UV reduction process.

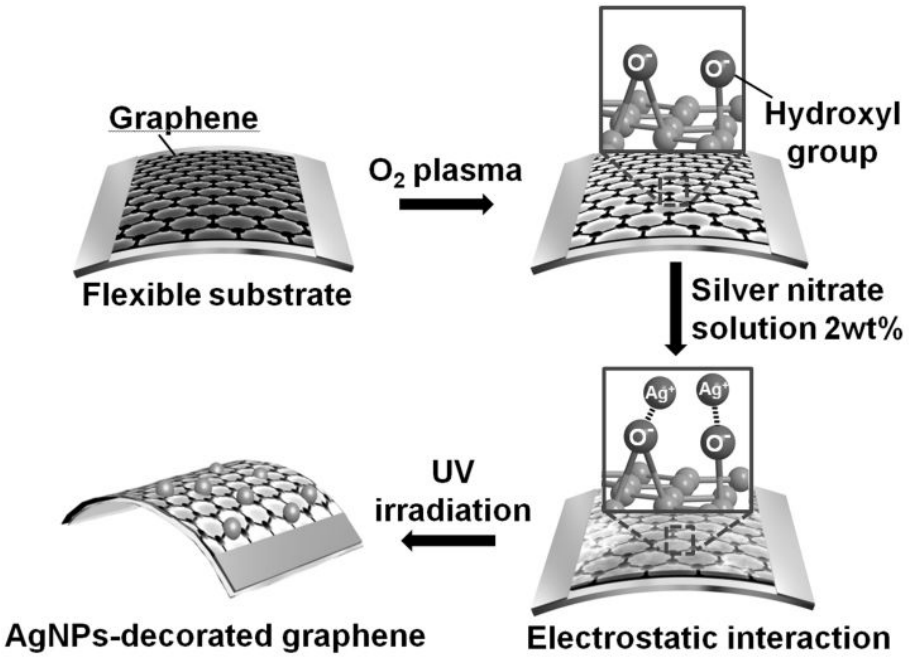

Figure. 7. Schematic illustration of AgNPs-G on flexible PET substrate.

3.2.1 Mechanism of AgNPs-G in photoreduction process

AgNPs-G was fabricated by dropping 2 wt% silver nitrate solutions onto the surface of the modified graphene and reducing AgNPs with UV irradiation. Oxygen atom in the functional groups on the OPFG is partially negative due to high electronegativity. Then, Silver ions with positive charge are easily attracted through electrostatic interactions and dispersed on the surface of the OPFG. Uniform Ag NPs were formed by a photoreduction process in a nucleation-growth mechanism [39, 40]. The Ag^{+} ions in silver nitrate solution act as nuclei for crystallization. These ions were reduced to elemental silver nanoparticles (Ag^{0}) by radicals of hydroxyl groups bonded to the graphene. UV light induced photolysis of the oxygen-containing functional groups and generated the radicals that assisted the reduction of silver ions in the graphene [42-44].

$$R\text{-}CH_2\text{-}OH \rightarrow R\text{-}CH^{\cdot}\text{-}OH + H^{\cdot} \quad (3)$$

$$Ag^{+} + R\text{-}CH^{\cdot}\text{-}OH \rightarrow Ag^{0} + R\text{-}COH + H^{+} \quad (4)$$

When Ag ions in aqueous solution were irradiated by UV light for 10 min, the photoreduced Ag NPs were formed with a uniform size distribution, *Ca.* 9 nm in diameter. Additionally, the thermal annealing process (above 100 ^{0}C for 6 h) was introduced for restoring the physical and electrical properties of the OPFG because the adsorbed or excess oxygen atoms diminished the conductivity of FLG [45]. Table 3 shows the atomic percentages of the elementary compositions before and after the thermal annealing process. The ratio of the oxygen atom decreased after the annealing process.

Table. 3 XPS atomic percentages of PG, OPFG 15, AgNPs-G 15, and annealed AgNPs-G 15.

Samples	C [%]	O [%]	Ag [%]
PG	76.44	22.86	-
OPFG 15	71.38	28.21	-
AgNPs-G 15	69.64	23.53	5.16
Annealing	73.64	19.86	5.74

3.2.2 AFM, XPS and TEM analysis of AgNPs-G film

The AgNPs-decorated graphene (AgNPs-G) was investigated by atomic force microscopy (AFM). Changes in roughness and thickness were monitored through AFM imaging. The surface of PG was smooth and uniform in figure 8. Additionally, the average thickness of the PG was *ca*. 2.8 nm, indicating FLG. It was found that thickness and roughness of AgNPs-G increased than those of PG in figure 8. The thickness of AgNPs-G 15 was 8 – 11 nm, and the diameter of the Ag NPs was confirmed to be *ca*. 7 - 9 nm. Considering these results, the Ag NPs were successfully adsorbed onto one side of the modified graphene [46].

The synthesis of AgNPs-G 15 was confirmed by the observation of XPS Ag 3d peaks [47]. The XPS pattern of AgNPs-G 15 was used to investigate the chemical state of the Ag NPs. The Ag 3d(5/2) and Ag 3d(3/2) bands appeared at binding energies of about 368.1 and 374.1 eV, respectively (Figure 9b). This energy splitting value of 6.0 eV indicates the formation of metallic Ag NPs. Moreover, the main

component of the synthesized nanoparticles was crystalline Ag^{0}.[35] Furthermore, increase of Ag loading was observed as a function of oxygen exposure time in figure 9a. The atomic percentage of Ag^{0} element increased from 2.86% in AgNPs-G 5 to 8.25% in AgNPs-G 20 owing to increase of the active sites to anchor the Ag metal nanoparticles.

To further clarify the surface and structure of AgNPs-G, Transmission electron microscopy (TEM) and high-resolution TEM (HR-TEM) were carried out. The Ag NPs reduced by UV-irradiation were homogeneously attached to the surface of the functionalized graphene (Figure 10). Well-dispersed Ag NPs were assembled on the surface of the OPFG, and the distribution of Ag NPs varied with the number of oxygen-containing functional groups bonded to the OPFG by simply changing the exposure time in figure 10. For AgNPs-G 5, the Ag NPs were sparsely decorated on the surface. Importantly, the distribution of Ag NPs increased with increasing the oxygen plasma exposure time, and there were considerable differences between

AgNPs-G 5 and AgNPs-G 20. Figure 10d shows that aggregation of Ag NPs occurred owing to the reaction of a large number of neighboring AgNPs with short interaction distance during UV reduction process [39, 48]. The HR-TEM image in figure 11 indicates that single-crystal Ag NPs (*ca*. 7 – 9 nm) were decorated on the OPFG (3 – 4 layers). The uniform size of the Ag NPs was controlled by UV-irradiation time and input power. In addition, the space fringe of the nanoparticles (inset in Figure 11) is *ca*. 0.23 nm which corresponds to the (111) lattice plane of Ag [49].

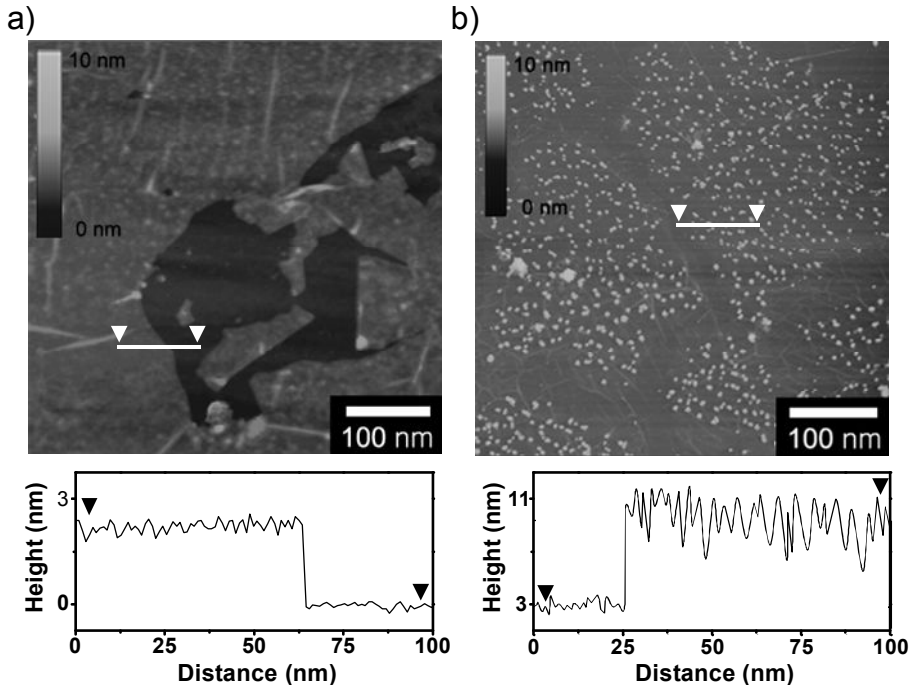

Figure. 8 AFM image of (a) PG with 2.8 nm in average thickness and (b) AgNPs-G 15 with thickness of 8-11 nm.

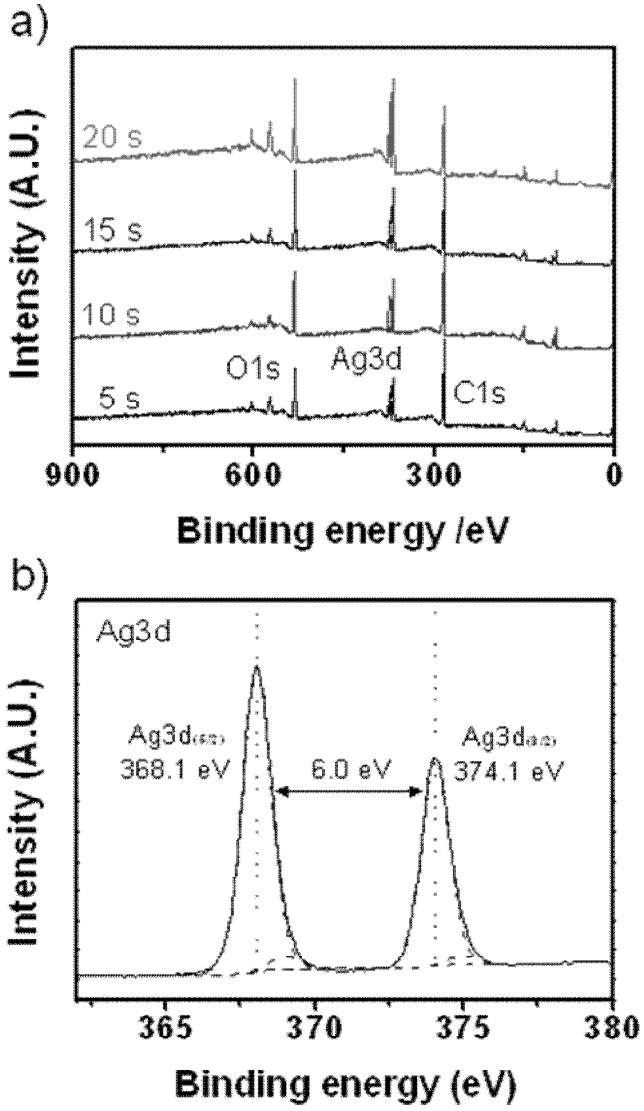

Figure. 9 XPS spectra of (a) various AgNPs-G as a function of plasma exposure time (5, 10, 15, and 20 s) and (b) high resolution Ag 3d for AgNPs-G 15.

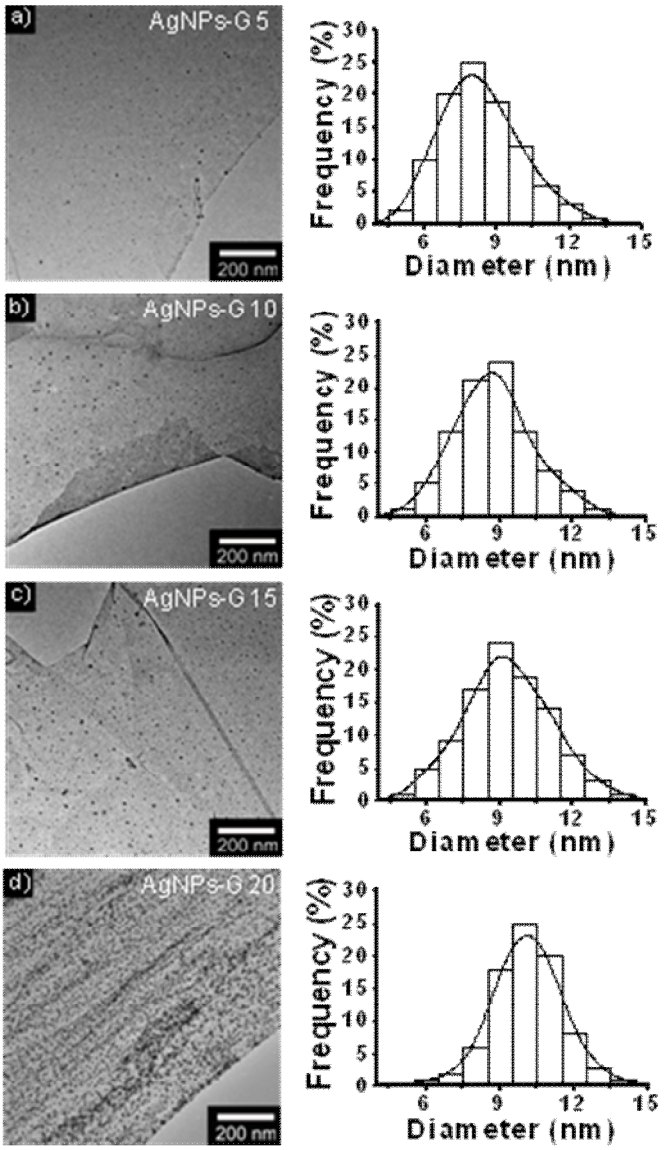

Figure. 10 TEM image and Ag NPs distribution diagram of (a) AgNPs-G 5.

(b) AgNPs-G 10, (c) AgNPs-G 15, and (d) AgNPs-G 20

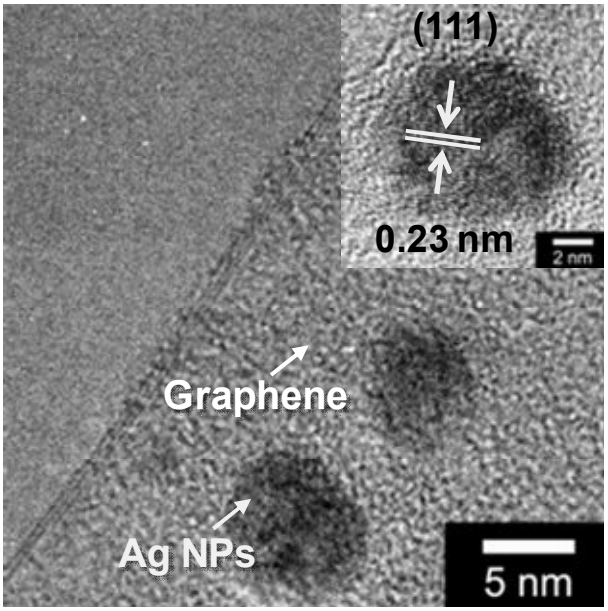

Figure. 11 HR-TEM image of Ag NPs (inset) and Ag NPs decorated few layered graphene. The size of the Ag NPs was *ca.* 8 nm.

3.2.3 Electrical and mechanical properties of AgNPs-G in a flexible system

Figure 12a illustrates the current-voltage (*I-V*) characteristics of Ag NPs-G transferred onto the flexible substrate as the conductive channel under bending system. The d*I*/d*V* value is the criterion used to establish how the graphene was affected by oxygen plasma treatment. The slope was *ca*. 4.72×10^{-4} for bent PG. The d*I*/d*V* value decreased with increasing plasma exposure time (3 to 20 s). Considering these results, a higher number of defects correspond to lower conductivities. The AgNPs-G 20 had an *I-V* curve with an extremely low slope, indicating that this material was not able to be used as a transducer of an electrical device due to absence of current flow. Moreover, the slope for bent AgNPs-G film is slightly lower than that for flat AgNPs-G film in figure 12b. Furthermore, the slope of the *I-V* curve of AgNPs-G decreased linearly with increasing plasma treatment time, signifying that the Ag NPs were effectively incorporated to functional groups on the surface of the graphene. The two *I-V* plots under

flexible and flat system are linear over a voltage range of – 1 to +1 V, representing the characteristic of ohmic contact [51, 52]. In this regard, this result provides reliable electrical contact at the interface between the AgNPs-G transducer and the gold electrode.

To manifest the mechanical flexibility of AgNPs-G, a bending experiment was conducted, and the resistance to bending was measured over different bending radii (3 to 12 mm). Although figure 13a displays a slight increase of resistance with smaller bending radius (from 12 to 3 mm), the largest resistance value has only a difference of *ca*. 1.2 % compared to its initial value at flat state. Furthermore, the original resistance was clearly restored after bending, which demonstrates excellent mechanical stability as a flexible transducer. In figure 13b, Fatigue test was demonstrated with flexible AgNPs-G film. The film resistance was shown to be stable after 90 bending cycles, and significant variation up to 100 bending cycles was not observed in inset of figure 13b. In addition, resistance ratio of AgNPs-G in initial state/ AgNPs-G after 100 bending cycles as was shown to be constant

from AgNPs-G 3 to AgNPs-G 15 film, whereas the resistance of AgNPs-G 20 slightly increased from original resistance in flat state by 19 % after 100 bending cycles. A possible explanation is that weak areas containing high level of defects and disorders in the graphene film might not survive at the tested bending cycles, resulting in low conductivity in AgNPs-G 20. However, the resistance variation of AgNPs-G film was generally consistent during the fatigue tests. From this point of view, the AgNPs-G as flexible transducer exhibited superior mechanical bendability, durability, and stability, leading to possibility for use of flexible electric device with sufficient robustness and high performance.

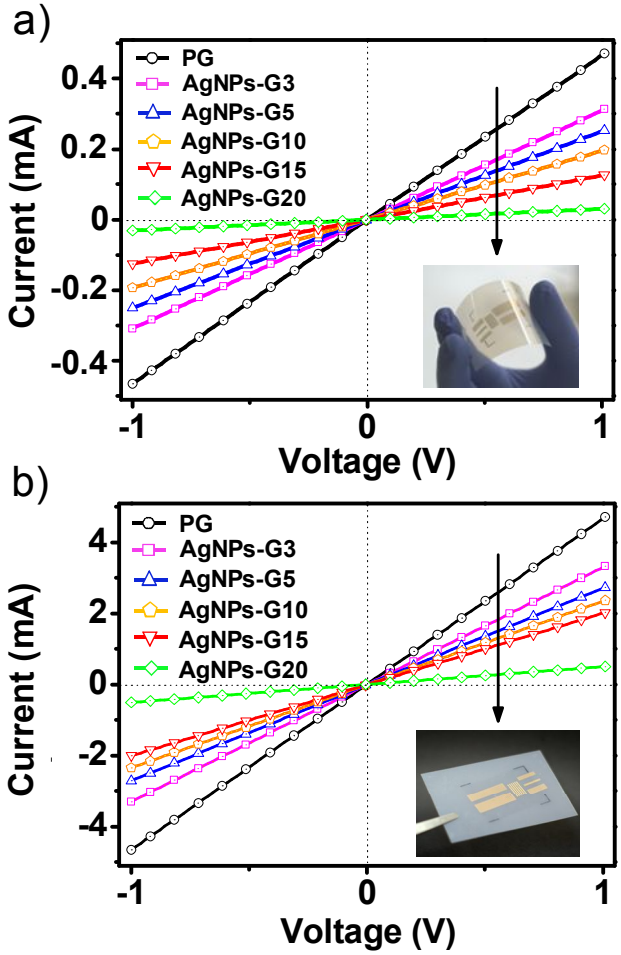

Figure. 12 Current-voltage (*I-V*) curves of PG and AgNPs-G (a) in flexible system and (b) in flat system based on the plasma-treated graphene with different time conditions (3, 5, 10, 15 and 20 s) in air circumstance Scan rate, V_{SD} = 0.1 V s^{-1} over a voltage range from -1 to +1 V.

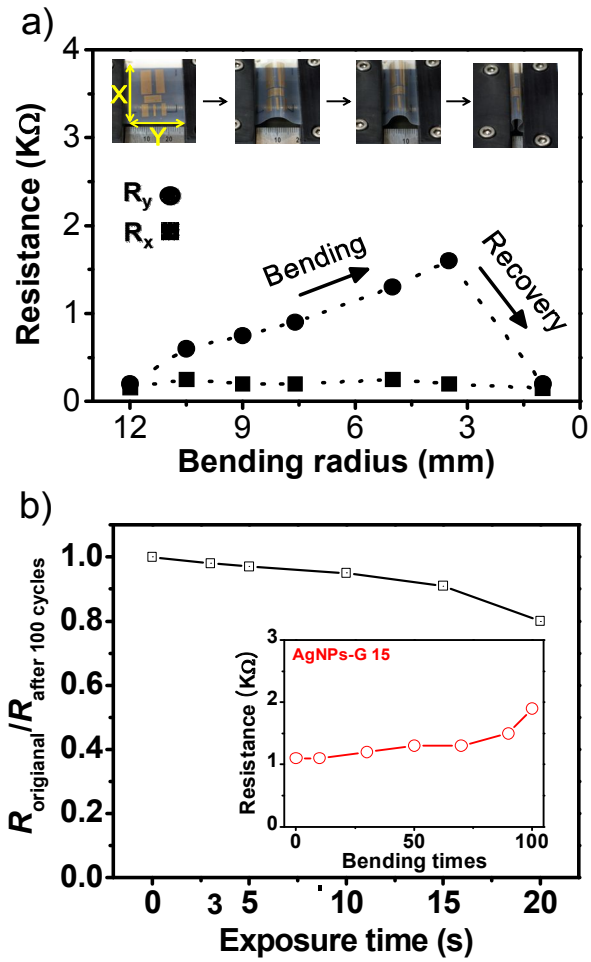

Figure. 13 (a) Variation in the resistance of flexible AgNPs-G 15 for different bending radii; inset exhibits the bending process. (b) Resistance ratio in flat system of AgNPs-G film treated by oxygen plasma for different exposure time. the resistance of the AgNPs-G 15, as a function of bending cycles up to 100 cycles (inset).

3.3 Application of AgNPs-G based flexible hydrogen sensor

Figure 14 shows the electrical response of AgNPs-G upon exposure to hydrogen gas with different concentrations. When AgNPs-G was exposed to H_2 gas at room temperature, resistance increased with rapid response time. However, a slow recovery time was observed owing to slow desorption of H_2 molecules from AgNPs-G at room temperature. Figure 14a illustrates the response of AgNPs-G upon sequential exposure to H_2 gas as a function of analyte concentration (40, 100, 200, 400, 600 and 800 ppm). The real-time responses were well-defined with increasing hydrogen gas concentrations, and then the AgNPs-G sensors showed reversible and reproducible real-time responses [52]. Their response times were less than 1 s for H_2 gas, and the recovery times were *ca*. 50 s for all AgNPs-G. The minimum detection level (MDL) of AgNPs-G15 was *ca*.40 ppm, approximately 1 - 2 orders of magnitude better than that of existing hydrogen sensors based on CVD graphene. This is attributed to high electron mobility

from the well-interconnected metal to the graphene. These response and recovery times are defined respectively as the required times for the gas sensor signals to reach 90% of the saturation value and then back to the original values [51, 52]. Moreover, the sensitivity of the AgNPs-G sensors increased with increasing amount of Ag NPs in the order: AgNPs-G5 < AgNPs-G10 < AgNPs-G15. Thus, a greater number of Ag NPs (present as acceptors) led to enhanced interactions with the analyte.

Figure 14b presents the real-time response of AgNPs-G upon periodic exposure to 200 ppm of H_2 gas. The cyclic tests demonstrated similar responses and excellent sensing performance over 10 cycles. AgNPs-G can be clearly used as a reversible material for detecting H_2 gas.

Figure 15 display the response of AgNPs-G sensor as a function of time and H_2 concentration under repeated bending/relaxing. No significant change was observed in the sensing behavior comparing with the result of flat AgNPs-G even if the sensitivity decreased from

initial value by only 4% after 100 bending cycles in H_2 200 ppm. Therefore, these results indicate that the AgNPs-G sensor exhibited superior mechanical bendability, durability, and stable sensing performance.

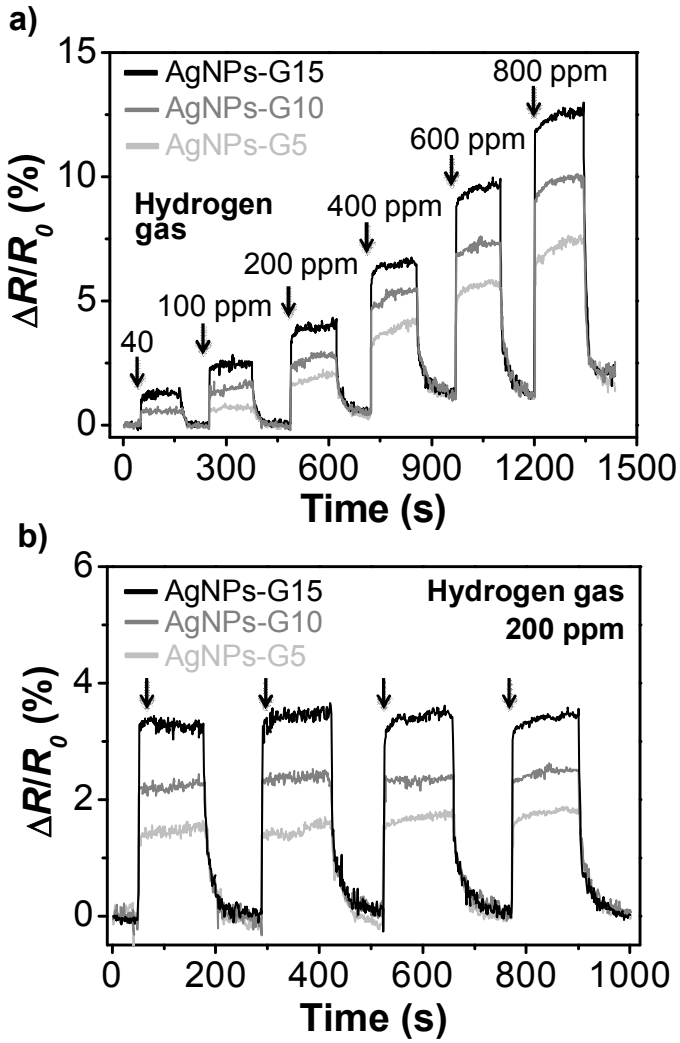

Figure. 14 Real-time response of AgNPs-G sensors measured at a constant current value (10^{-5}A). Normalized resistance changes upon (a) sequential exposure to H_2 gas (40, 100, 200, 400, 600 and 800 ppm) and (b) periodic exposure to H_2 gas of 200 ppm.

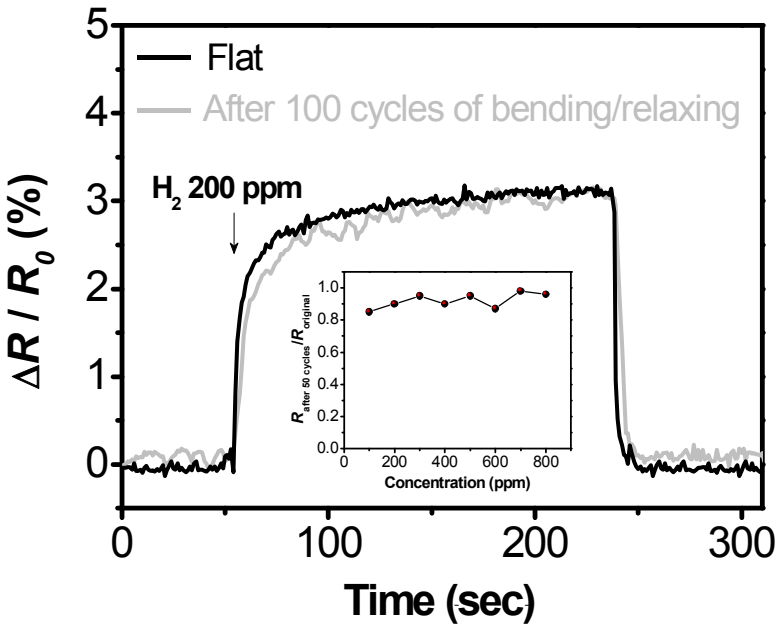

Figure. 15 The sensing behavior of AgNPs-G sensor toward H_2 200 ppm after 100 cycles of bending/relaxing. Inset exhibits fatigue test toward various H_2 concentrations.

Chapter 4. Conclusion

In conclusion, the surface of CVD-grown few-layer graphene was successfully functionalized by oxygen plasma-based surface engineering with variation of exposure time, input power and distance. Various oxygen-containing functional groups bonded to the OPFG surface react with silver ions under UV irradiation as external reduction source, leading to AgNPs-G nanocomposites. Moreover, as exposure time (5, 10, 15 and 20 s) in O_2 plasma increased, the loading amount of uniform Ag nanoparticles increased in the order of AgNPs-G 5 < AgNPs-G 10 < AgNPs-G 15 < AgNPs-G 20. Furthermore, a flexible AgNPs-G transducer has superior mechanical bendability and durability, which opens up the possibility applying to electronic devices.

As the electronic application, the AgNPs-G hydrogen sensors had a tendency to increase sensitivity with increasing plasma exposure duration in the order AgNPs-G5 < AgNPs-G10 < AgNPs-G15. The

MDL of AgNPs-G15 was *ca*. 40 ppm. The response time was less than 1 s, and the recovery time decreased gradually with increasing Ag NPs population. This could realize the potential of fabricating flexible hydrogen sensors for commercial applications.

References

[1] B. Wang, X.-L. Wu, C.-Y. Shu, Y.-G. Guo, C.-R. Wang, *J. Mater. Chem.*, 2010, **20**, 10661-10664.

[2] D. Wang, R. Kou, D. Choi, Z. Yang, Z. Nie, J. Li, L. V. Saraf, D. Hu, J. Zhang, G. L. Graff, J. Liu, M. A. Pope, I. A. Aksay, *ACS Nano*, 2010, **4**, 1587-1595.

[3] C. Xu, X. Wang, J. Zhu, *J. Phys. Chem. C*, 2008, **112**, 19841-19845

[4] S. Guo, S. Dong, E. Wang, *ACS Nano*, 2010, **4**, 547-555.

[5] C. Song, D. Wu, F. Zhang, P. Liu, Q. Lu, X. Feng, *Chem. Commun*, 2012, **48**, 2119-2121.

[6] J. S. Kim, J. H. Yun, I. Kim, S. E. Shim, *Jounal of Industrial and Engineering Chemistry*, 2011, **17**, 325-330

[7] G. Goncalves, P. A. A. P. Marques, C. M. Granadeiro, H. I. S. Nogueira, M. K. Singh, J. Gracio, *Chem. Mater.*, 2009, **21**, 4796-4802.

[8] X. Lu, H. Qi, X. Zhang, Z. Xue, J. Jin, X. Zhou, X. Liu, *Chem. Commun.*, 2011, **47**, 12494-12496

[9] S. Park, K.-S. Lee, G. Bozoklu, W. Cai, S. T. Nguyen, R. S. Ruoff, *ACS Nano*, 2008, **2**, 572-578

[10] K. S. Kim, Y. Zhao, H. Jang, S. Y. Lee, J. M. Kim, K. S. Kim, J.-H. Ahn, P. Kim, J.-Y. Choi, B. H. Hong, *Nature,* 2009, **457**, 706-710.

[11] W. J. Yu, S. H. Chae, S. Y. Lee, D. L. Duong, Y. H. Lee, *Adv. Mater.,* 2011, **23**, 1889-1893.

[12] S. Stankovich, D. A. Dikin, G. H. B. Dommett, K. M. Kohlhaas, E. J. Zimney, E. A. Stach, R. D. Piner, S. T. Nguyen, R. S. Ruoff, *nature*, 2006, **442**, 282-286

[13] C. Liu, K. Wang, S. Luo, Y. Tang, L. Chen, *small*, **7**, 1203-1206

[14]. R.-H. Kim, M.-H. Bae, D. G. Kim, H. Cheng, B. H. Kim, D.-H. Kim, M. Li, J. Wu, F. Du, H.-S. Kim, *Nano Lett.*, 2011, **11**, 3881-3886

[15] A. Venugopal, L. Colombo, E. M. Vogel, *Appl. Phys. Lett.*, 2010, **96**, 013512.

[16] S.-H. Baeck, T. F. Jaramillo, G. D. stucky, E. W. McFarland, *Chem. Mater.*, 2003, **15**, 3411-3413

[17] Y. Xia, N. Venkateswaran, D. Qin, J. Tien, G. M. Whitesides, *Langmuir*,

1998, **14**, 363-371.

[18] X.-W. Liu, J.-J. Mao, P.-D. Liu, X.-W. Wei, *Carbon*, 2011, **49**, 477.

[19] A. Gutes, B. Hsia, A. Sussman, W. Mickelson, A. Zettl, C. Carraro, R. Maboudian, *Nanoscale*, 2012, **4**, 438.

[20] R. Zan, U. Bangert, Q. Ramasse, K. S. Novoselove, J. Phys. Chem. Lett., 2012, 3, 953-958

[21] A. Geroge, T. M. Stawski, S. Unnikrishnan, S. A. Veldhuis, J. E. t. Elshof, *J. mater. Chem.*, 2012, **22**, 328

[22] I.-S. Hwang, J.-K. Choi, H.-S. Woo, S.-J. Kim, S.-Y. Jung, T.-Y. Seong, I.-D. Kim, J.-H. Lee, *ACS Appl. Mater. Interfaces,* 2011, **3**, 3140-3145.

[23] Z. Zhang, F. Xu, W. Yang, M. Guo, X. Wang, B. Zhang, J. Tang, *Chem. Commun.,* 2011, **47**, 6440-6442.

[24] V. Hrachova, A. Kaoka, *Vacuum*, 1997, **48**, 689

[25] C. Chen, B. Liang, A. Ogino, X. Wang, M. Nagatsu, *J. Phys. Chem. C*, 2009, **113**, 7659-7665.

[26] T. Tang, N. Lu, J. K. Wang, S. K. Ryu, H. S. Choi, *J. Phys. Chem. C*, 2007, **111**, 1820.

[27] R. Larciprete, S. Fabris, T. Sun, P. Lacovig, A. Baraldi, S. Lizzit, *J. Am. Chem. Soc.,* 2011, **133**, 17315-17321.

[28] M, L, Steen, C. I. Butoi, E. R. Fisher, *Langmuir*, 2001, **17**, 81566.

[29] A. C. Ferrari, J. C. Meyer, V. Scardaci, C. Casiraghi, M. Lazzeri, F. Mauri, S. Piscanec, D. Jiang, K. S. Novoselov, S. Roth, A. K. Geim, *Phys. Rev. Lett.,* 2006, **97**, 187401.

[30] D. Long, J.–Y. Hong, W. Li, J. Miyawaki, L. Ling, I. Mochida, S.-H. Yoon, J. Jang, *ACS Nano,* 2011, **5**, 6254-6261

[31] C. Casiraghi, A. Hartschuh, H. Qian, S. Piscanec, C. Georgi, A. Fasoli, K. S. Novoselov, D. M. Basko, A. C. Ferrari, *Nano Lett.,* 2009, **9**, 1433-1441.

[32] J. Chen, Y. Wen, Y. Guo, B. Wu, L. Huang, Y. Xue, D. Geng, D. Wang, G. Yu, Y. Liu, *J. Am. Chem. Soc.,* 2011, **133**, 17548-17551.

[33] D. C. kim, D.-Y. Jeon, H.-J. Chung, Y. Woo, J. K. Shin, S. Seo, *Nanotechnology*, 2009, 20, 375703

[34] Q. Li, Z. Li, M. Chen, Y. Fang, *Nano Lett.,* 2009, **9**, 2129-2132.

[35] H.-W. Tien, Y.-L. Huang, S.-Y. Yang, J.-Y. Wang, C.-C. M. Ma, *Carbon,* 2011, **49**, 1550-1560.

[36] W. Chen, X. Liu, Y. Lin, Y. Bang, H. I. Kim, *Jounal of Industrial and Engineering Chemistry*, 2011, **17**, 455-460

[37] H. S. Suh, H. Kang, C.-C. Liu, P. F. Nealey, K. Char, *Macromolecules*, 2010, **43**, 461-466.

[38] Y. J. Shin, Y. Wang, H. Huang, G. Kalon, A. T. S. Wee, Z. Shen, C. S. Bhatia, H. Yang, *Langmuir*, 2010, **26**, 3798-3802.

[39] D. Cheng, X. Zhou, H. Xia, H. S. O. Chan, *Chem. Mater.,* 2005, **17**, 3578-3581.

[40] G. Williams, B. Seger, P. V. Kamat, *ACS Nano,* 2008, **2**, 1487-1491.

[41] R. Pasricha, S. Gupta, A. G. Joshi, N. Bahadur, D. Haranathe, K. N. Sood, S. Singh, S. Singh, materialstoday, 2012, 15, 118-125.

[42] O. Akhavan, M. Abdolahad, Y. Abdi, S. Mohajerzadeh, *J. Mater. Chem.,* 2011, **21**, 387-393.

[43] H. Hada, Y. Yonezawa, A. Yoshida, A. Kurakake, *J. Phys. Chem.,* 1976, **80**, 2728-2731.

[44] M. Harada, E. Katagiri, *Langmuir,* 2010, **26**, 17896-17905.

[45] Z. Jin, T. P. McNicholas, C.-J. Shih, Q. H. Wang, G. L. C. Paulus, A. J.

Hilmer, S. Shimizu, M. S. Strano, *Chem. Mater.,* 2011, **23**, 3362-3370

[46] C. Xu, X. Wang, J. Zhu, *J. Phys. Chem. C,* 2008, **112**, 19841-19845.

[47] W. Ren, Y. Fang, E. Wang, *ACS Nano,* 2011, **5**, 6425-6433.

[48] K. Mallik, M. Mandal, N. Pradhan, T. Pal, *Nano. Lett.*, 2001, **1**, 319-322.

[49] P.-Y. Silvert, H.-U. Ronaldo, T.-E. Kamar, *J. Mater. Chem.*, 1997, **7**, 293-299.

[50] O. S. Kwon, S. J. Park, J.-Y. Hong, A.-R. Han, J. S. Lee, J. S. Lee, J. H. Oh, J. Jang, *ACS Nano*, 2012, **6**, 1486-1493.

[51] H. Yoon, J. Jang, *Adv. Funct. Mater.,* 2009, **19**, 1567-1576.

[52] J. S. Lee, O. S. Kwon, S. J. Park, E. Y. Park, S. A. You, H. Yoon, J. Jang, *ACS Nano,* 2011, **5**, 7992-8001.

[53] Y-G Zhou, J-J Chen, F.-B. Wang, Z.-H. Sheng, X.-H. Xia, *Chem. Commun*, 2010, **46**, 5951-5953.

초 록

화학기상증착 방법으로 제조된 그래핀을 산소 플라즈마를 통하여 표면 개질 하고, 초 박막 그래핀/메탈 나노복합체를 제조하여 플렉서블 센서에 응용하였다. 산소 플라즈마는 노출시간, 전압, 그리고 그래핀과 플라즈마 전극의 높이차이를 변수로 두어, 그래핀의 관능기의 수를 조절하였다. 뿐만 아니라, 높은 표면에너지를 갖는 개질화된 그래핀에 은 메탈이온을 자외선에 유도된 환원방법을 통하여 부착하였고, 플라즈마 노출 시간을 증가시킴에 따라 그래핀/메탈 복합체 내의 메탈입자의 분포도 또한 증가하였다. 이와 같이 제조된 그래핀/메탈 나노 복합체 박막은 우수한 기계적 강도와 유연성을 갖고, 플렉서블 수소센서에 성공적으로 응용될 수 있었으며 그 결과, 상온에서 가역적이고 높은 센서 성능을 보임을 확인할 수 있었다.

주요어: 그래핀 나노복합체, 화학기상증착 제조, 산소 플라즈마, 플렉서블 그래핀 센서.

학번: 2011-21050